A univariate approximation at most probable point for higher-order reliability analysis

S. Rahman [*], D. Wei

Department of Mechanical and Industrial Engineering, The University of Iowa, Iowa City, IA 52242, United States

Abstract

This paper presents a new univariate method employing the most probable point as the reference point for predicting failure probability of structural and mechanical systems subject to random loads, material properties, and geometry. The method involves novel decomposition at the most probable point that facilitates a univariate approximation of a general multivariate function, response surface generation of the univariate function, and Monte Carlo simulation. In addition to the effort of identifying the most probable point, the method requires a small number of exact or numerical evaluations of the performance function at selected input. Results of four numerical examples involving elementary mathematical functions and structural/solid-mechanics problems indicate that the proposed method provides accurate and computationally efficient estimates of probability of failure. Finally, the fatigue failure of lever arm in a wheel loader has been evaluated, demonstrating the ability of the new method in solving industrial-scale fatigue reliability problems.
© 2005 Elsevier Ltd. All rights reserved.

Keywords: Reliability; Decomposition methods; Most probable point; Univariate approximation; Response surface; Probabilistic fracture; Stochastic fatigue

1. Introduction

A fundamental problem in time-invariant component reliability analysis entails calculation of a multi-fold integral (Madsen et al., 1986; Rackwitz, 2001; Ditlevsen and Madsen, 1996)

[*] Corresponding author. Tel.: +1 319 335 5679; fax: +1 319 335 5669.
E-mail address: rahman@engineering.uiowa.edu (S. Rahman).
URL: http://www.engineering.uiowa.edu/~rahman (S. Rahman).

$$P_{\mathrm{F}} \equiv P[g(\boldsymbol{X}) < 0] = \int_{g(\boldsymbol{x})<0} f_{\mathbf{X}}(\boldsymbol{x})\,\mathrm{d}\boldsymbol{x}, \tag{1}$$

where $\boldsymbol{X} = \{X_1, \ldots, X_N\}^{\mathrm{T}} \in \mathbb{R}^N$ is a real-valued, N-dimensional random vector defined on a probability space $(\Omega, \mathscr{F}, P)$ comprising the sample space Ω, the σ-field $\mathscr{F}$, and the probability measure P; $g(\boldsymbol{x})$ is the performance function, such that $g(\boldsymbol{x}) < 0$ represents the failure domain; P_{F} is the probability of failure; and $f_{\mathbf{X}}(\boldsymbol{x})$ is the joint probability density function of $\boldsymbol{X}$, which typically represents loads, material properties, and geometry. For most practical problems, the exact evaluation of this integral, either analytically or numerically, is not possible because N is large, $f_{\mathbf{X}}(\boldsymbol{x})$ is generally non-Gaussian, and $g(\boldsymbol{x})$ is highly non-linear function of $\boldsymbol{x}$.

The most common approach to compute the failure probability in Eq. (1) involves the first- and second-order reliability methods (FORM/SORM) (Madsen et al., 1986; Rackwitz, 2001; Ditlevsen and Madsen, 1996; Breitung, 1984; Hohenbichler et al., 1987; Cai and Elishakoff, 1994; Tvedt, 1990; Der Kiureghian and Dakessian, 1998), which are based on linear (FORM) or quadratic approximation (SORM) of the limit-state surface at a most probable point (MPP). Experience has shown that FORM/SORM are sufficiently accurate for engineering purposes, provided that the limit-state surface at the MPP is close to being linear or quadratic, and no multiple MPPs exist. For highly non-linear performance functions, which exist in many structural problems, results based on FORM/SORM must be interpreted with caution. If the Rosenblatt transformation, frequently used to map non-Gaussian random input into its standard Gaussian image, yields a highly non-linear limit state, inadequate reliability estimates by FORM/SORM may result (Bjerager, 1988; Nie and Ellingwood, 2000). Furthermore, the existence of multiple MPPs could give rise to large errors in standard FORM/SORM approximations (Ditlevsen and Madsen, 1996; Der Kiureghian and Dakessian, 1998). In that case, multi-point FORM/SORM along with the system reliability concept is required for improving component reliability analysis (Der Kiureghian and Dakessian, 1998).

Recently, the authors have developed new decomposition methods, which can solve highly non-linear reliability problems more accurately or more efficiently than FORM/SORM and simulation methods (Xu and Rahman, accepted for publication). A major advantage of these decomposition methods, so far based on mean point of random input as a reference point, over FORM/SORM is that higher-order approximations of performance functions can be achieved without calculating MPP or gradients. However, for certain class of reliability problems existing methods may require computationally demanding higher-variate (bivariate, trivariate, etc.) decomposition to adequately represent performance functions. Hence, developing univariate methods, capable of producing computationally efficient, yet sufficiently adequate performance functions, is a major motivation of the current work.

This paper presents a new MPP-based univariate method for predicting reliability of mechanical systems subject to random loads, material properties, and geometry. Section 2 presents a novel decomposition technique that facilitates a lower-dimensional approximation of a general multivariate function. Section 3 describes response surface generation of the univariate approximation. Section 4 utilizes the Monte Carlo simulation using response surface models embedded in the reliability method. Four numerical examples involving elementary mathematical functions and structural problems illustrate the proposed method in Section 5. Comparisons have been made with alternative approximate and simulation methods to evaluate the accuracy and computational efficiency of the new method. Finally, an industrial-scale, fatigue reliability problem is solved in Section 6 using the proposed univariate method.

2. Multivariate function decomposition at MPP

Consider a continuous, differentiable, real-valued performance function $g(\boldsymbol{x})$ that depends on $\boldsymbol{x} = \{x_1, \ldots, x_N\}^{\mathrm{T}} \in \mathbb{R}^N$. The transformed limit states $h(\boldsymbol{u}) = 0$ and $y(\boldsymbol{v}) = 0$ are the maps of the original limit state $g(\boldsymbol{x}) = 0$ in the standard Gaussian space ($\boldsymbol{u}$ space) and the rotated Gaussian space ($\boldsymbol{v}$ space), respectively,
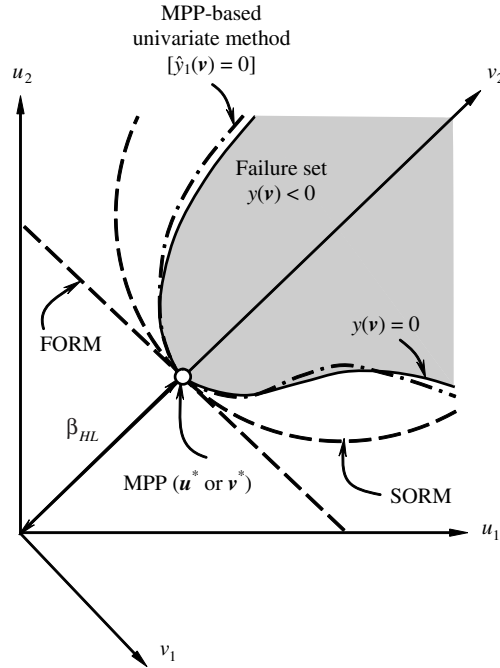
Fig. 1. Performance function approximations by various methods.

as shown in Fig. 1 for $N = 2$. The closest point on the limit-state surface to the origin, denoted by the MPP (u^* or v^*) or beta point, has a distance β_{HL}, which is commonly referred to as the Hasofer–Lind reliability index (Madsen et al., 1986; Rackwitz, 2001; Ditlevsen and Madsen, 1996). The determination of MPP and β_{HL} involves standard non-linear constrained optimization and is usually performed in the standard Gaussian space. Fig. 1 depicts FORM and SORM approximations of the limit-state surface at MPP.

Suppose that $y(v)$ has a convergent Taylor series expansion at MPP $v^* = \{v_1^*, \ldots, v_N^*\}^{\mathrm{T}}$ and can be expressed by

$$y(v) = y(v^*) + \sum_{j=1}^{\infty} \frac{1}{j!} \sum_{i=1}^{N} \frac{\partial^j y}{\partial v_i^j}(v^*)(v_i - v_i^*)^j + \mathscr{R}_2 \tag{2}$$

or

$$y(v) = y(v^*) + \sum_{j=1}^{\infty} \frac{1}{j!} \sum_{i=1}^{N} \frac{\partial^j y}{\partial v_i^j}(v^*)(v_i - v_i^*)^j + \sum_{j_1, j_2 > 0}^{\infty} \frac{1}{j_1! j_2!} \sum_{i_1 < i_2} \frac{\partial^{j_1+j_2} y}{\partial v_{i_1}^{j_1} \partial v_{i_2}^{j_2}}(v^*)(v_{i_1} - v_{i_1}^*)^{j_1}(v_{i_2} - v_{i_2}^*)^{j_2} + \mathscr{R}_3, \tag{3}$$

where the remainder $\mathscr{R}_2$ denotes all terms with dimension two and higher and the remainder $\mathscr{R}_3$ denotes all terms with dimension three and higher.

2.1. Univariate approximation

Consider a univariate approximation of $y(v)$, denoted by

$$\hat{y}_1(v) \equiv \hat{y}_1(v_1, \ldots, v_N) = \sum_{i=1}^{N} y(v_1^*, \ldots, v_{i-1}^*, v_i, v_{i+1}^*, \ldots, v_N^*) - (N-1)y(v^*), \tag{4}$$

where each term in the summation is a function of only one variable and can be subsequently expanded in a Taylor series at $v = v^*$, yielding

$$\hat{y}_1(v) = y(v^*) + \sum_{j=1}^{\infty} \frac{1}{j!} \sum_{i=1}^{N} \frac{\partial^j y}{\partial x_i^j}(v^*)(v_i - v_i^*)^j. \tag{5}$$

Comparison of Eqs. (2) and (5) indicates that the univariate approximation leads to the residual error $y(v) - \hat{y}_1(v) = \mathscr{R}_2$, which includes contributions from terms of dimension two and higher. For sufficiently smooth $y(v)$ with convergent Taylor series, the coefficients associated with higher-dimensional terms are usually much smaller than that with one-dimensional terms. As such, higher-dimensional terms contribute less to the function, and therefore, can be neglected. Nevertheless, Eq. (4) includes all higher-order univariate terms, as compared with FORM and SORM, which only retain linear and quadratic terms, respectively. Hence, $\hat{y}_1(v)$ yields more accurate representation of $y(v)$ than FORM/SORM. Furthermore, Eq. (4) represents exactly the same function as $y(v)$ when $y(v) = \sum y_i(v_i)$, i.e., when $y(v)$ can be additively decomposed into functions $y_i(v_i)$ of single variables.

2.2. Bivariate approximation

In a similar manner, consider a bivariate approximation

$$\hat{y}_2(v) = \sum_{i_1 < i_2} y(v_1^*, \ldots, v_{i_1-1}^*, v_{i_1}, v_{i_1+1}^*, \ldots, v_{i_2-1}^*, v_{i_2}, v_{i_2+1}^*, \ldots, v_N^*) - (N-2)$$
$$\times \sum_{i=1}^{N} y(v_1^*, \ldots, v_{i-1}^*, v_i, v_{i+1}^*, \ldots, v_N^*) + \frac{(N-1)(N-2)}{2} y(v^*) \tag{6}$$

of $y(v)$, where each term on the right-hand side is a function of at most two variables and can be expanded in a Taylor series at $v = v^*$, yielding

$$\hat{y}_2(v) = y(v^*) + \sum_{j=1}^{\infty} \frac{1}{j!} \sum_{i=1}^{N} \frac{\partial^j y}{\partial v_i^j}(v^*)(v_i - v_i^*)^j + \sum_{j_1, j_2 > 0}^{\infty} \frac{1}{j_1! j_2!} \sum_{i_1 < i_2} \frac{\partial^{j_1 + j_2} y}{\partial v_{i_1}^{j_1} \partial v_{i_2}^{j_2}}(v^*)(v_{i_1} - v_{i_1}^*)^{j_1}(v_{i_2} - v_{i_2}^*)^{j_2}. \tag{7}$$

Again, the comparison of Eqs. (3) and (7) indicates that the bivariate approximation leads to the residual error $y(v) - \hat{y}_2(v) = \mathscr{R}_3$, in which the remainder $\mathscr{R}_3$ includes terms of dimension three and higher. The bivariate approximation includes all terms with no more than two variables, thus yielding higher accuracy than the univariate approximation. Furthermore, Eq. (6) exactly represents $y(v) = \sum \sum y_{ij}(v_i, v_j)$, i.e., when $y(v)$ can be additively decomposed into functions $y_{ij}(v_i, v_j)$ of at most two variables.

2.3. Generalized S-variate approximation

The procedure for univariate and bivariate approximations described in the preceding can be generalized to an S-variate approximation for any integer $1 \leqslant S \leqslant N$. The generalized S-variate approximation of $y(v)$ is

$$\hat{y}_S(v) \equiv \sum_{i=0}^{S} (-1)^i \binom{N-S+i-1}{i} \sum_{k_1 < \cdots < k_{S-i}} y(v_1^*, \ldots, v_{k_1-1}^*, v_{k_1}, v_{k_1+1}^*, \ldots, v_{k_{S-i}-1}^*, v_{k_{S-i}}, v_{k_{S-i}+1}^*, \ldots, v_N^*).$$
$$\tag{8}$$

If $y_R \equiv y(v_1^*, \ldots, v_{k_1-1}^*, v_{k_1}, v_{k_1+1}^*, \ldots, v_{k_R-1}^*, v_{k_R}, v_{k_R+1}^*, \ldots, v_N^*); 0 \leqslant R \leqslant S$, a multivariate function decomposition theorem, developed by the first author's group, leads to (Xu and Rahman, 2004)

$$y_R = \sum_{k=0}^{R} \binom{N-k}{R-k} t_k; \quad 0 \leqslant R \leqslant S, \tag{9}$$

where

$$t_0 = y(\mathbf{v}^*)$$

$$t_1 = \sum_{j_1} \frac{1}{j_1!} \sum_{i_1=1}^{N} \frac{\partial^{j_1} y}{\partial v_{i_1}^{j_1}}(\mathbf{v}^*)(v_{i_1} - v_{i_1}^*)^{j_1}$$

$$t_2 = \sum_{j_1,j_2} \frac{1}{j_1!j_2!} \sum_{i_1<i_2} \frac{\partial^{j_1+j_2} y}{\partial v_{i_1}^{j_1} \partial v_{i_2}^{j_2}}(\mathbf{v}^*)(v_{i_1} - v_{i_1}^*)^{j_1}(v_{i_2} - v_{i_2}^*)^{j_2} \tag{10}$$

$$\vdots$$

$$t_S = \sum_{j_1,\ldots,j_S} \frac{1}{j_1! \cdots j_S!} \sum_{i_1<\cdots<i_S} \frac{\partial^{j_1+\cdots+j_S} y}{\partial v_{i_1}^{j_1} \cdots \partial v_{i_S}^{j_S}}(\mathbf{v}^*)(v_{i_1} - v_{i_1}^*)^{j_1} \cdots (v_{i_S} - v_{i_S}^*)^{j_S}$$

Using Eqs. (9) and (10), it can be shown that $\hat{y}_S(\mathbf{v})$ in Eq. (8) consists of all terms of the Taylor series of $y(\mathbf{v})$ that have less than or equal to S variables (Xu and Rahman, 2004). The expanded form of Eq. (8), when compared with the Taylor expansion of $y(\mathbf{v})$, indicates that the residual error in the S-variate approximation is $y(\mathbf{v}) - \hat{y}_S(\mathbf{v}) = \mathcal{R}_{S+1}$, where the remainder $\mathcal{R}_{S+1}$ includes terms of dimension $S+1$ and higher. When $S = 1$, Eq. (8) degenerates to the univariate approximation (Eq. (4)). When $S = 2$, Eq. (8) becomes the bivariate approximation (Eq. (6)). Similarly, trivariate, quadrivariate, and other higher-variate approximations can be derived by appropriately selecting the value of S. In the limit, when $S = N$, Eq. (8) converges to the exact function $y(\mathbf{v})$. In other words, the decomposition technique generates a convergent sequence of approximations of $y(\mathbf{v})$.

2.4. Remarks

The decomposition of a general multivariate function $y(\mathbf{v})$ can be viewed as a finite sum

$$y(\mathbf{v}) = \underbrace{\underbrace{\underbrace{y_0 + \sum_{i=1}^{N} y_i(v_i)}_{=\hat{y}_1(\mathbf{v})} + \sum_{\substack{i_1,i_2=1 \\ i_1<i_2}}^{N} y_{i_1 i_2}(v_{i_1}, v_{i_2})}_{=\hat{y}_2(\mathbf{v})} + \cdots + \sum_{\substack{i_1,\ldots,i_S=1 \\ i_1<\cdots<i_S}}^{N} y_{i_1\cdots i_S}(v_{i_1}, \ldots, v_{i_S})}_{=\hat{y}_S(\mathbf{v})}$$

$$+ \cdots + y_{12\cdots N}(v_1, \ldots, v_N), \tag{11}$$

where y_0 is a constant, $y_i(v_i)$ is a univariate component function representing independent contribution to $y(\mathbf{v})$ by input variable v_i acting alone, $y_{i_1 i_2}(v_{i_1}, v_{i_2})$ is a bivariate component function describing cooperative influence of two input variables v_{i_1} and v_{i_2}, $y_{i_1,\ldots,i_S}(v_{i_1}, \ldots, v_{i_S})$ is an S-variate component function quantifying cooperative effects of S input variables $v_{i_1}, \ldots, v_{i_S}$, and so on. By comparing Eqs. (4) and (6) with Eq. (11), the univariate and bivariate approximations provide two- and three-term approximants, respectively, of the finite decomposition. In general, the S-variate approximation in Eq. (8) yields the $S + 1$-term approximant of the decomposition. The fundamental conjecture underlying this work is that component functions arising in the proposed decomposition will exhibit insignificant higher-dimensional effects cooperatively.

It is worth noting that the univariate approximation in Eq. (4) should not viewed as first- or second-order Taylor series expansions nor does it limit the non-linearity of $y(\boldsymbol{v})$. According to Eq. (5), *all* higher-order univariate terms of $y(\boldsymbol{v})$ are included in the proposed approximation. In fact, the univariate component function $y_i(v_i)$ can be highly non-linear and therefore should provide in general higher-order representation of a performance function than those by FORM or SORM. Furthermore, the approximations contain contributions from *all* input variables.

Finally, the decomposition presented here depends on the selected reference point. It is elementary to show that an improper or careless selection of the reference point can spoil the approximation. The authors' past work indicates that the mean point of random input is a good candidate for defining the reference point (Xu and Rahman, accepted for publication). This present work is motivated by the argument that using MPP as the reference point may provide an improved function approximation, however, with the additional expense of identifying the MPP.

3. Response surface generation

Consider the univariate component function $y_i(v_i) \equiv y(v_1^*, \ldots, v_{i-1}^*, v_i, v_{i+1}^*, \ldots, v_N^*)$ in Eq. (4). If for $v_i = v_i^{(j)}$, n function values

$$y_i(v_i^{(j)}) = y(v_1^*, \ldots, v_{i-1}^*, v_i^{(j)}, v_{i+1}^*, \ldots, v_N^*); \quad j = 1, 2, \ldots, n \tag{12}$$

are given, the function value for arbitrary v_i can be obtained using the Lagrange interpolation as

$$y_i(v_i) = \sum_{j=1}^{n} \phi_j(v_i) y_i(v_i^{(j)}), \tag{13}$$

where the shape function $\phi_j(v_i)$ is defined as

$$\phi_j(v_i) = \frac{\prod_{k=1, k\neq j}^{n}(v_i - v_i^{(k)})}{\prod_{k=1, k\neq j}^{n}(v_i^{(j)} - v_i^{(k)})}. \tag{14}$$

By using Eqs. (13) and (14), arbitrarily many values of $y_i(v_i)$ can be generated if n values of that component function are given. The same procedure is repeated for all univariate component functions, i.e., for all $y_i(v_i)$, $i = 1, \ldots, N$. Therefore, the total cost for the univariate approximation in Eq. (4), in addition to that required for locating MPP, entails a *maximum* of $nN + 1$ function evaluations.

More accurate bivariate or multivariate approximations (e.g., Eqs. (6) or (8)) can be developed in a similar way. However, because of much higher cost of multivariate approximations, only the univariate approximation will be examined in this paper.

4. Monte Carlo simulation

For component reliability analysis, the Monte Carlo estimate $P_{F,1}$ of the failure probability employing the proposed univariate approximation is

$$P_{F,1} = \frac{1}{N_S} \sum_{i=1}^{N_S} \mathscr{I}[\hat{y}_1(\boldsymbol{v}^{(i)}) < 0], \tag{15}$$

where $\boldsymbol{v}^{(i)}$ is the ith realization of $\boldsymbol{V}$, N_S is the sample size, and $\mathscr{I}[\cdot]$ is an indicator function such that $\mathscr{I} = 1$ if $\boldsymbol{v}^{(i)}$ is in the failure set (i.e., when $\hat{y}_1(\boldsymbol{v}^{(i)}) < 0$) and *zero* otherwise. Similar failure probability estimates can

be developed using higher-variate models if required. In addition, similar approximations can be employed for system reliability analysis (Xu and Rahman, accepted for publication).

The decomposition method involving univariate approximation (Eq. (4)), *n*-point Lagrange interpolation (Eqs. (13) and (14)), and Monte Carlo simulation (Eq. (15)) is defined as the *MPP-based univariate method* in this paper. Since the univariate method leads to explicit response-surface approximation of a performance function, the embedded Monte Carlo simulation can be conducted for any sample size. However, the accuracy and efficiency of the resultant failure-probability calculation depend on both the univariate and response surface approximations. They will be evaluated using several numerical examples, as follows.

5. Numerical examples

Four numerical examples involving explicit performance functions from mathematical or solid-mechanics problems (Examples 1 and 2) and implicit performance functions from structural or solid-mechanics problems (Examples 3 and 4), are presented to illustrate the MPP-based univariate method developed. Whenever possible, comparisons have been made with existing mean-point-based univariate method, FORM/SORM, and Monte Carlo simulation methods to evaluate the accuracy and computational efficiency of the proposed method. For the MPP-based univariate method, n (=3, 5, 7 or 9) uniformly distributed points $v_i^* - (n-1)/2, v_i^* - (n-3)/2, \ldots, v_i^*, \ldots, v_i^* + (n-3)/2, v_i^* + (n-1)/2$ were deployed at the v_i-coordinate, leading to $(n-1)N + 1$ function evaluations in addition to those required for locating the MPP.

When comparing computational efforts by various methods, the number of *original* performance function evaluations is chosen as the primary metric in this paper. For the direct Monte Carlo simulation, the number of original function evaluations is the same as the sample size. However, in univariate methods, they are different, because the Monte Carlo simulation (although with same sample size as in direct Monte Carlo simulation) embedded in the proposed method is conducted using their response surface approximations. The difference in CPU times in evaluating an original function and its response surface approximation is significant when a calculation of the original function involves expensive finite-element analysis, as in Examples 3 and 4. However, the difference becomes trivial when analyzing explicit performance functions, as in Examples 1 and 2. Hence, the computational effort expressed in terms of function evaluations alone should be carefully interpreted for explicit performance functions. Nevertheless, the number of function evaluations provides an objective measure of the computational effort for reliability analysis of realistic problems.

5.1. Example 1—elementary mathematical functions

Consider a cubic and a quartic performance functions (Grandhi and Wang, 1999), expressed respectively by

$$g(X_1, X_2) = 2.2257 - \frac{0.025\sqrt{2}}{27}(X_1 + X_2 - 20)^3 + \frac{33}{140}(X_1 - X_2) \tag{16}$$

and

$$g(X_1, X_2) = \frac{5}{2} + \frac{1}{216}(X_1 + X_2 - 20)^4 - \frac{33}{140}(X_1 - X_2), \tag{17}$$

where $X_i \mapsto N(10, 3^2)$, $i = 1, 2$ are independent, Gaussian random variables, each with mean $\mu = 10$ and standard deviation $\sigma = 3$. From an MPP search, $\mathbf{v}^* = \{0, 2.2257\}^T$ and $\beta_{HL} = \|\mathbf{v}^*\| = 2.2257$ for the cubic function and $\mathbf{v}^* = \{0, 2.5\}^T$ and $\beta_{HL} = \|\mathbf{v}^*\| = 2.5$ for the quartic function, as shown in Figs. 2(a) and (b),
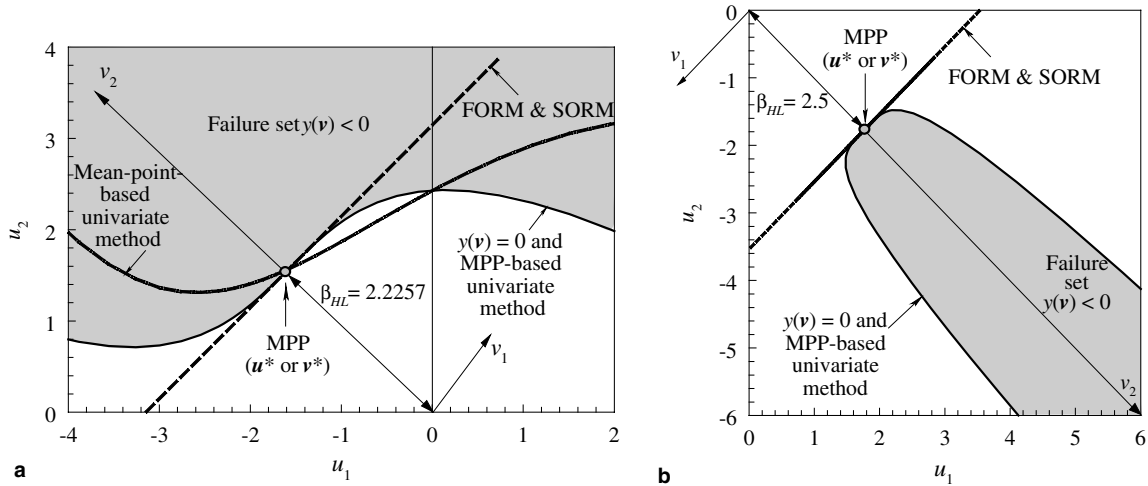
Fig. 2. Approximate performance functions by various methods: (a) cubic function; (b) quartic function.

respectively. In addition, Figs. 2(a) and (b) plots exact limit-state surfaces and their various approximations by FORM/SORM (Breitung, 1984; Hohenbichler et al., 1987; Cai and Elishakoff, 1994), mean-point-based univariate method (Xu and Rahman, accepted for publication), and proposed MPP-based univariate method. For univariate methods, a value of $n = 5$ was selected, resulting nine function evaluations. According to Figs. 2(a) and (b), the MPP-based univariate method yields exact limit-state equations, since both performance functions considered are univariate functions and at most consist of fourth-order polynomial in the rotated Gaussian space. For the cubic function, the limit-state equation by the mean-point-based univariate method matches the exact equation only at MPP. However, for the quartic function, the mean-point-based limit-state equation is non-negative, leading to a null failure set. FORM and SORM yield grossly inaccurate representation of both limit-state equations, due to zero (inflection point of the cubic function) or very small (highly non-linearity of the quartic function) curvatures at MPP.

Tables 1 and 2 show the results of the failure probability calculated by FORM, SORM due to Breitung (1984), Hohenbichler et al. (1987) and Cai and Elishakoff (1994), mean-point-based univariate method (Xu and Rahman, accepted for publication), proposed MPP-based univariate method, and direct Monte Carlo simulation using 10^6 samples. The MPP-based univariate method predicts exact probability of failure. The

Table 1
Failure probability for cubic performance function

Method	Failure probability	Number of function evaluations[a]
MPP-based univariate method	0.01907	29[b]
Mean-point-based univariate method (Xu and Rahman, accepted for publication)	0.01558	9[c]
FORM	0.01302	21
SORM (Breitung, 1984)	0.01302	204
SORM (Hohenbichler et al., 1987)	0.01302	204
SORM (Cai and Elishakoff, 1994)	0.01302	204
Direct Monte Carlo simulation	0.01907	1,000,000

[a] Total number of times the original performance function is calculated.
[b] $21 + (n-1) \times N = 21 + (5-1) \times 2 = 29$.
[c] $(n-1) \times N + 1 = (5-1) \times 2 + 1 = 9$.

Table 2
Failure probability for quartic performance function

Method	Failure probability	Number of function evaluations[a]
MPP-based univariate method	0.002886	29[b]
Mean-point-based univariate method (Xu and Rahman, accepted for publication)	0.0	_[c]
FORM	0.006209	21
SORM (Breitung, 1984)	0.006208	212
SORM (Hohenbichler et al., 1987)	0.006208	212
SORM (Cai and Elishakoff, 1994)	0.006206	212
Direct Monte Carlo simulation	0.002886	1,000,000

[a] Total number of times the original performance function is calculated.
[b] $21 + (n-1) \times N = 21 + (5-1) \times 2 = 29$.
[c] Not applicable.

univariate method using mean point, which yields poor approximations of performance functions [see Figs. 2(a) and (b)], underpredicts failure probability (cubic function) or fails to provide a solution (quartic function). Other commonly used reliability methods, such as FORM and SORM, underpredict failure probability by 31% and overpredict failure probability by 117% when compared with the direct Monte Carlo results. The SORM results are the same as the FORM results, indicating that there is no improvement over FORM for problems involving inflection points or high nonlinearity.

5.2. Example 2—burst margin of a rotating disk

Consider an annular disk of inner radius R_i, outer radius R_o, and constant thickness $t \ll R_o$ (plane stress), as shown in Fig. 3. The disk is subject to an angular velocity ω about an axis perpendicular to its plane at the center. The maximum allowable angular velocity ω_a when tangential stresses through the thickness reach the material ultimate strength S_u factored by a material utilization factor α_m is (Boresi and Schmidt, 2003)

$$\omega_a = \left[\frac{3\alpha_m S_u (R_o - R_i)}{\rho(R_o^3 - R_i^3)} \right]^{1/2}, \tag{18}$$
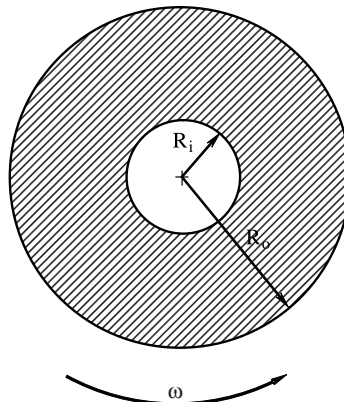

Fig. 3. Rotating annular disk subject to angular velocity.

where ρ is the mass density of the material. According to an SAE G-11 standard, the satisfactory performance of the disk is defined when the burst margin M_b, defined as

$$M_b \equiv \frac{\omega_a}{\omega} = \left[\frac{3\alpha_m S_u (R_o - R_i)}{\rho \omega^2 (R_o^3 - R_i^3)} \right]^{1/2} \tag{19}$$

exceeds a critical threshold of 0.37473 (Penmetsa and Grandhi, 2003). If random variables $X_1 = \alpha_m$, $X_2 = S_u$, $X_3 = \omega$, $X_4 = \rho$, $X_5 = R_o$, and $X_6 = R_i$, and have their statistical properties defined in Table 3, the performance function becomes

$$g(\boldsymbol{X}) = M_b(X_1, X_2, X_3, X_4, X_5, X_6) - 0.37473. \tag{20}$$

Table 4 presents predicted failure probability of the disk and associated computational effort using MPP-based univariate method, mean-point-based univariate and bivariate methods (Xu and Rahman, accepted for publication), FORM, Hohenbichler's SORM (Hohenbichler et al., 1987), and direct Monte Carlo simulation (10^6 samples). For univariate and bivariate methods, a value of $n = 7$ was selected. The results indicate that the proposed MPP-based univariate method and mean-point-based bivariate method produce the most accurate solution. The mean-point-based univariate method significantly overpredicts the failure probability, whereas FORM and SORM slightly underpredict the failure probability. The MPP-based univariate method surpasses the efficiency of both SORM and mean-point-based bivariate method in solving this particular reliability problem.

Table 3
Statistical properties of random input for rotating disk

Random variable	Mean	Standard deviation	Probability distribution
α_m	0.9377	0.0459	Weibull[a]
S_u, ksi	220	5	Gaussian
ω, rpm	24	0.5	Gaussian
ρ, lb s^2/in^4	0.29/g[b]	0.0058/g[b]	Uniform[c]
R_o, in	24	0.5	Gaussian
R_i, in	8	0.3	Gaussian

[a] Scale parameter = 25.508; shape parameter = 0.958.
[b] $g = 385.82$ in/s^2.
[c] Uniformly distributed over $(0.28, 0.3)$.

Table 4
Failure probability of rotating disk

Method	Failure probability	Number of function evaluations[a]
MPP-based univariate method	0.00101	167[b]
Mean-point-based univariate method (Xu and Rahman, accepted for publication)	0.00159	37[c]
Mean-point-based bivariate method (Xu and Rahman, accepted for publication)	0.00103	577[d]
FORM	0.000894	131
SORM (Hohenbichler et al., 1987)	0.000970	378
Direct Monte Carlo simulation	0.00104	1,000,000

[a] Total number of times the original performance function is calculated.
[b] $131 + (n-1) \times N = 131 + (7-1) \times 6 = 167$.
[c] $(n-1) \times N + 1 = (7-1) \times 6 + 1 = 37$.
[d] $N \times (N-1) \times (n-1)^2/2 + (n-1) \times N + 1 = 6 \times (6-1) \times (7-1)^2/2 + (7-1) \times 6 + 1 = 577$.

5.3. Example 3–10-bar truss structure

A 10-bar, linear-elastic, truss structure, shown in Fig. 4, was studied in this example to examine the accuracy and efficiency of the proposed reliability method. The Young's modulus of the material is 10^7 psi. Two concentrated forces of 10^5 lb are applied at nodes 2 and 3, as shown in Fig. 4. The cross-sectional area X_i, $i = 1,\ldots,10$ for each bar follows truncated normal distribution clipped at $x_i = 0$ and has mean $\mu = 2.5$ in^2 and standard deviation $\sigma = 0.5$ in^2. According to the loading condition, the maximum displacement $[(v_3(X_1,\ldots,X_{10})]$ occurs at node 3, where a permissible displacement is limited to 18 in. Hence, the performance function is

$$g(X) = 18 - v_3(X_1,\ldots,X_{10}). \tag{21}$$

From the MPP search involving finite-difference gradients, the reliability index is $\beta_{\mathrm{HL}} = \|v^*\| = 1.3642$. Table 5 shows the failure probability of the truss, calculated using the proposed MPP-based univariate method, mean-point based univariate method (Xu and Rahman, accepted for publication), FORM, three
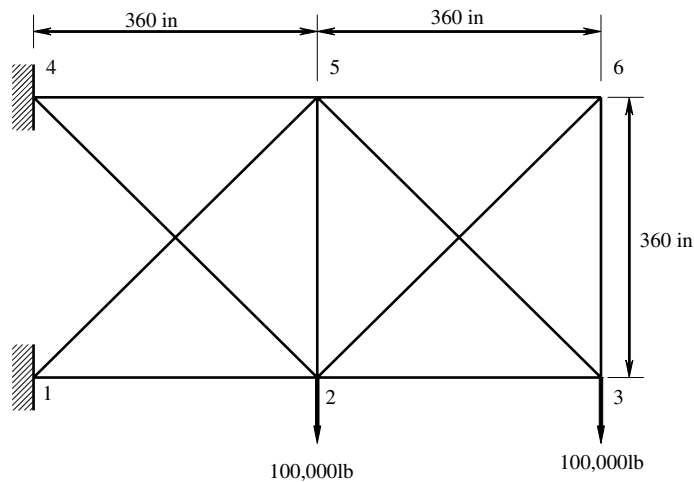

Fig. 4. A 10-bar truss structure.

Table 5
Failure probability of 10-bar truss structure

Method	Failure probability	Number of function evaluations[a]
MPP-based univariate method	0.1465	187[b]
Mean-point-based univariate method (Xu and Rahman, accepted for publication)	0.1357	61[c]
FORM	0.0862	127
SORM (Breitung, 1984)	0.1286	506
SORM (Hohenbichler et al., 1987)	0.1524	506
SORM (Cai and Elishakoff, 1994)	0.1467	506
Direct Monte Carlo simulation	0.1394	1,000,000

[a] Total number of times the original performance functions is calculated.

[b] $127 + (n-1) \times N = 127 + (7-1) \times 10 = 187$.

[c] $(n-1) \times N + 1 = (7-1) \times 10 + 1 = 61$.

variants of SORM due to Breitung (1984), Hohenbichler et al. (1987) and Cai and Elishakoff (1994), and direct Monte Carlo simulation (10^6 samples). For univariate methods, a value of $n = 7$ was selected. As can be seen from Table 5, both versions of the univariate method predict the failure probability more accurately than FORM and all three variants of SORM. This is because univariate methods are able to approximate the performance function more accurately than FORM and SORM. A comparison of the number of function evaluations, also listed in Table 5, indicates that the mean-point-based univariate method is the most efficient method. The number of function evaluations by the MPP-based univariate method is slightly larger than FORM, but much less than SORM.

5.4. Example 4—mixed-mode fracture-mechanics analysis

The final example involves an isotropic, homogeneous, edge-cracked plate, presented to illustrate mixed-mode probabilistic fracture-mechanics analysis using the proposed univariate method. As shown in Fig. 5(a), a plate of length $L = 16$ units, width $W = 7$ units is fixed at the bottom and subjected to a far-field and a shear stress τ^∞ applied at the top. The elastic modulus and Poisson's ratio are 1 unit and 0.25, respectively. A plane strain condition was assumed. The statistical property of the random input $X = \{a/W, \tau^\infty, K_{Ic}\}^T$ is defined in Table 6.

Due to the far-field shear stress τ^∞, the plate is subjected to mixed-mode deformation involving fracture modes I and II (Anderson, 1995). The mixed-mode stress-intensity factors $K_I(X)$ and $K_{II}(X)$ were calculated using an interaction integral method (Yau et al., 1980). The plate was analyzed using the finite element method (FEM) involving a total of 832 8-noded, regular, quadrilateral elements and 48 6-noded, quarter-point (singular), triangular elements at the crack-tip, as shown in Fig. 5(b).
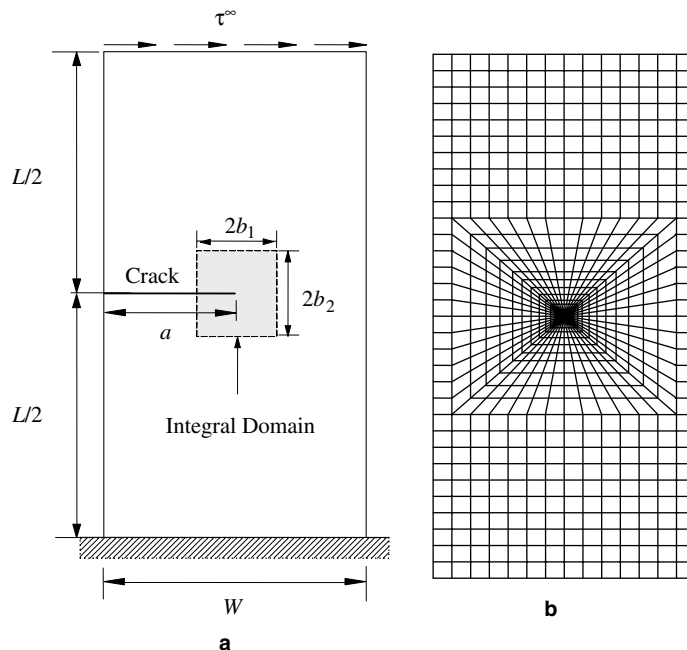

Fig. 5. An edge-cracked plate subject to mixed-mode deformation: (a) geometry and loads; (b) finite-element discretization.

Table 6
Statistical properties of random input for an edge-cracked plate

Random variable	Mean	Standard deviation	Probability distribution
a/W	0.5	0.2309	Uniform[a]
τ^{∞}	Variable[b]	0.1	Gaussian
K_{Ic}	200	0.1	Lognormal

[a] Uniformly distributed over (0.3, 0.7).
[b] Varies from 2.6 to 3.1.

The failure criterion is based on a mixed-mode fracture initiation using the maximum tangential stress theory (Anderson, 1995), which leads to the performance function

$$g(\mathbf{X}) = K_{Ic} - \left[K_I(\mathbf{X})\cos^2\frac{\Theta(\mathbf{X})}{2} - \frac{3}{2}K_{II}(\mathbf{X})\sin\Theta(\mathbf{X}) \right]\cos\frac{\Theta(\mathbf{X})}{2}, \tag{22}$$

where K_{Ic} is statistically distributed fracture toughness, typically measured from small-scale fracture experiments under mode I and plane strain conditions, and $\Theta_c(\mathbf{X})$ is the direction of crack propagation, given by

$$\Theta_c(\mathbf{X}) = \begin{cases} 2\tan^{-1}\left(\dfrac{1 - \sqrt{1 + 8[K_{II}(\mathbf{X})/K_I(\mathbf{X})]^2}}{4K_{II}(\mathbf{X})/K_I(\mathbf{X})} \right), & \text{if } K_{II}(\mathbf{X}) > 0, \\[4mm] 2\tan^{-1}\left(\dfrac{1 + \sqrt{1 + 8[K_{II}(\mathbf{X})/K_I(\mathbf{X})]^2}}{4K_{II}(\mathbf{X})/K_I(\mathbf{X})} \right), & \text{if } K_{II}(\mathbf{X}) < 0. \end{cases} \tag{23}$$

Failure probability estimates of $P_F = P[g(\mathbf{X}) < 0]$, obtained using the proposed MPP-based univariate method, mean-point-based univariate and bivariate methods, FORM, Hohenbeichler's SORM, and direct Monte Carlo simulation, are compared in Fig. 6 and are plotted as a function of $\mathbb{E}[\tau^{\infty}]$, where $\mathbb{E}$ is the expectation operator. For each reliability analysis (i.e., each point in the plot), FORM and SORM require 29 and 42 function evaluations (finite-element analysis). Using $n = 9$, the mean-point-based and MPP-
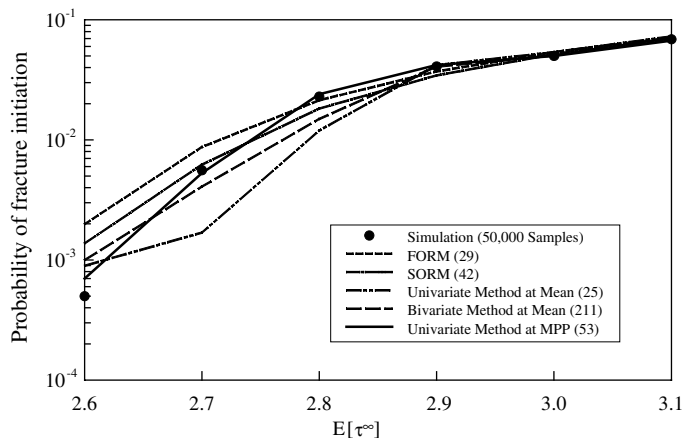

Fig. 6. Probability of fracture initiation in an edge-cracked plate.

based univariate methods require only 25 and 53 (=29 + 24) function evaluations, respectively, whereas 211 and 50,000 finite-element analyses are needed by the mean-point-based bivariate method and Monte Carlo simulation, respectively. The results clearly show that MPP-based univariate method is more accurate than other methods, particularly when the failure probability is low. The computational effort by MPP-based univariate method is much lower than that by mean-point-based bivariate or simulation methods.
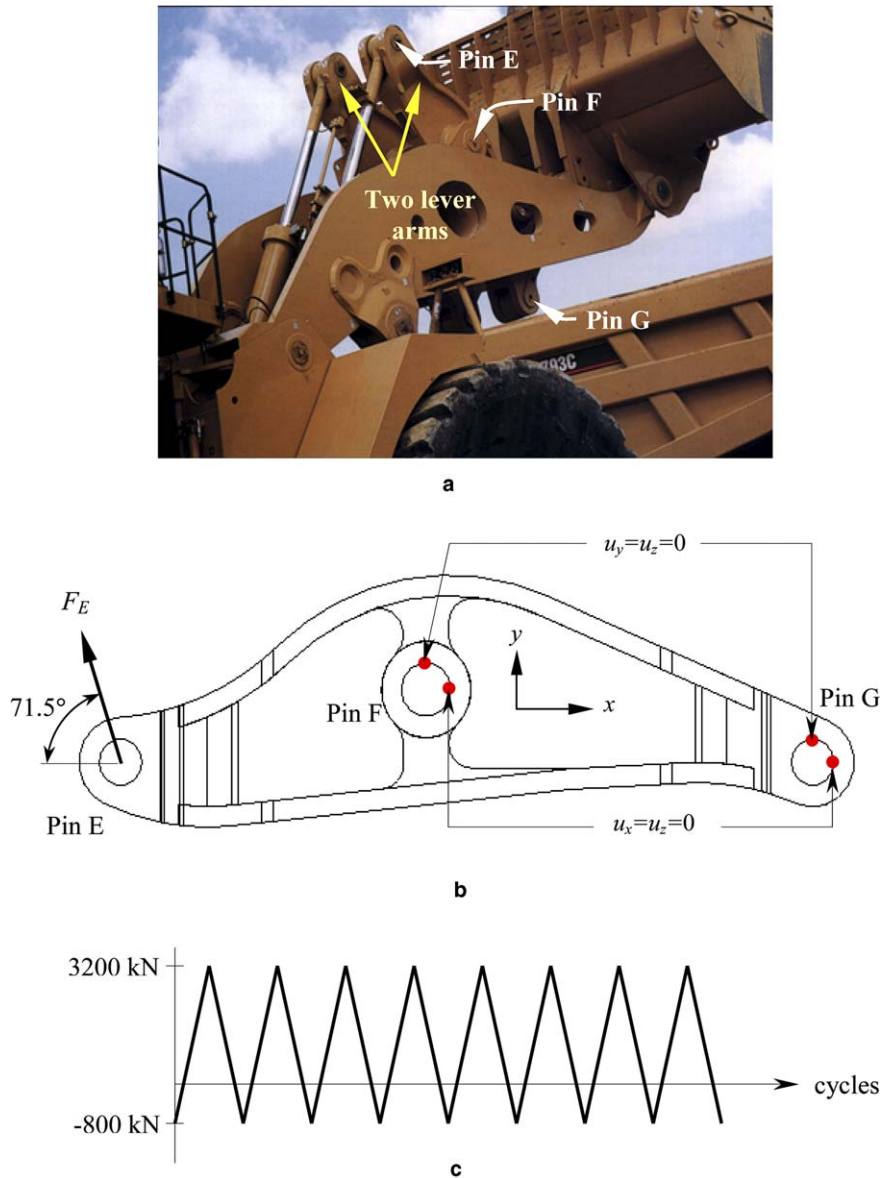

Fig. 7. A wheel loader under cyclic loads: (a) two lever arms; (b) loading and boundary conditions of a lever arm; (c) constant-amplitude cyclic loads at pin E.

6. Fatigue reliability application

The objective of this section is to illustrate the effectiveness of the proposed univariate method in solving a large-scale practical engineering problem. The problem involves mechanical fatigue durability and reliability analyses of a lever arm in a wheel loader.

6.1. Problem definition and input

Fig. 7(a) shows a wheel loader commonly used in the heavy construction industry. A major structural problem entails fatigue life evaluation of lever arms, also depicted in Fig. 7(a). The loading and boundary conditions of a single lever arm are shown in Fig. 7(b). The load F_E at pin E can be viewed as an input load due to other mechanical components of the wheel loader. The deterministic constant-amplitude load cycles at pin E vary from -800 to 3200 kN and are shown in Fig. 7(c). The lever arm is made of cast steel with deterministic elastic properties, as follows: (1) Young's modulus $E = 203$ GPa, (2) Poisson's ratio $v = 0.3$. In general, the random input vector X, which comprises casting defect characteristics and material properties, include defect radius r, ultimate strength S_u, fatigue strength coefficient σ'_f, fatigue strength exponent b, fatigue ductility coefficient ε'_f, and fatigue ductility exponent c. Table 7 defines statistical properties of X. The objective is to predict fatigue durability and reliability of the lever arm. A value of $n = 3$ was selected for the proposed univariate method.

6.2. Fatigue reliability analysis

The von Mises strain-life method was employed for fatigue durability analysis (Stephens et al., 2001). According to this method, the Coffin–Manson–Morrow equation for determining fatigue crack-initiation life N_f at a point is (Stephens et al., 2001).

$$\frac{\Delta \varepsilon}{2} = \frac{\sigma'_f - \sigma_m}{E}(2N_f)^b + \varepsilon'_f(2N_f)^c, \tag{24}$$

where $\Delta \varepsilon$ is the equivalent strain range and σ_m is the equivalent mean stress, both of which depend on strain and stress fields. Appendix A provides a brief exposition of calculating $\Delta \varepsilon$ and σ_m, which requires results of linear-elastic finite-element stress analysis. Appendix B describes how defect size can be estimated from casting simulation.

Table 7
Statistical properties of random input for lever arm

Random variable[a]	Mean	Coefficient of variation	Probability distribution
σ'_f, MPa	1332	0.1	Lognormal
b	-0.1085	0.1	Lognormal
ε'_f	0.375	0.1	Lognormal
c	-0.6354	0.1	Lognormal
S_u, MPa	847	0.05	Lognormal
r, mm	Variable[b]	0.1	Lognormal

[a] Random variables S_u and r are active only when casting defects are considered.
[b] Varies as follows: 14.4, 5.5, and 11.5 mm at locations 1, 2, and 3, respectively (see Fig. 10).

Once $\Delta\varepsilon$ and σ_m are determined, the fatigue life $N_f(X)$, which depends on random input X, can be calculated by solving Eq. (24). The fatigue failure is defined when $N_f(X)$ is less than a design threshold n_0, leading to a performance function
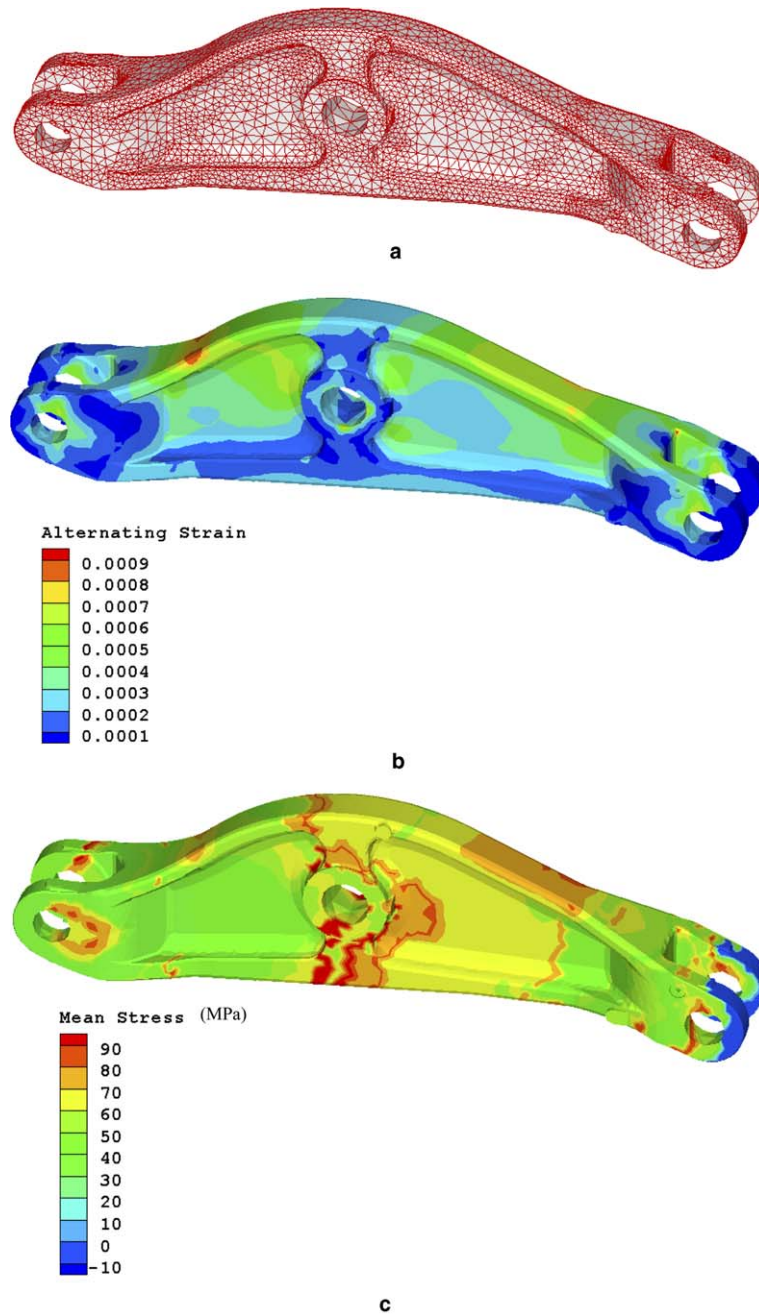
Fig. 8. Finite element analysis of a lever arm: (a) mesh (77,154 elements; 17,089 nodes); (b) equivalent alternating strain ($\Delta\varepsilon/2$) contour; (c) equivalent mean stress (σ_m) contour.

$$g(\boldsymbol{X}) = N_{\mathrm{f}}(\boldsymbol{X}) - n_0. \tag{25}$$

A value of $n_0 = 10^7$ cycles was employed in this study.

6.3. Results

6.3.1. Without defects

Fig. 8(a) shows a three-dimensional finite-element mesh of the lever arm involving 77,154 tetrahedral elements and 17,089 nodes, which was generated using the ABAQUS commercial software (ABAQUS, 2002). Using the FEM-based stress analysis and following the procedure described in Appendix A, Fig. 8(b) and (c) presents contours of equivalent alternating strain (=half of equivalent strain range = $\Delta\varepsilon/2$) and equivalent mean stress (σ_{m}), respectively, of the lever arm.

The MPP-based univariate method was applied to calculate the probability of fatigue failure $P_{\mathrm{F}} \equiv P[N_{\mathrm{f}}(\boldsymbol{X}) < n_0]$. Since no defects are considered initially, only four random variables comprising fatigue strength coefficient, fatigue strength exponent, fatigue ductility coefficient, and fatigue ductility exponent are required. Fig. 9 shows the contour plot of the reliability index $\beta \equiv \Phi^{-1}(1 - P_{\mathrm{F}})$ of the entire lever arm. Results indicate that the reliability indices are relatively small (i.e., failure probabilities are relatively large) in Region A where there are large strains [see Fig. 8(a)] or in Region B where there are large mean stress [see Fig. 8(b)] and are expected. A further comparative analysis indicates that largest failure probabilities in Regions A and B are 0.0127 and 0.00466, respectively. Therefore, if the lever arm is redesigned, a natural tendency is to modify the shape or size of Region A until the failure probability is lowered to a target value.

6.3.2. With defects

The probabilistic analysis described in the preceding can also be employed when casting-induced shrinkage defects are considered. However, any detrimental effect of defect size on $\Delta\varepsilon$ and σ_{m} and two additional random variables, such as defect radius and ultimate strength S_{u}, (see Appendix A) must be accounted for
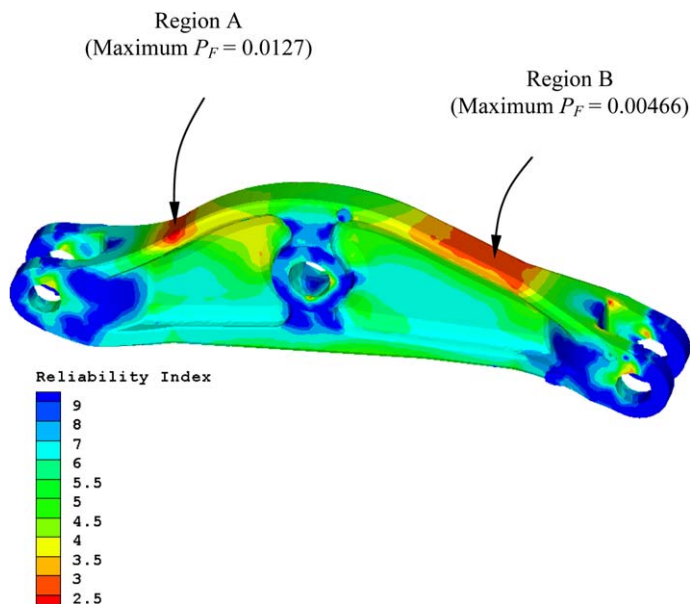

Fig. 9. Fatigue life-based reliability index contour of lever arm.

in subsequent reliability analysis. Fig. 10 shows the contour plot of porosity distribution in the lever arm and was generated using the MAGMASOFT commercial software (MAGMASOFT, 2002). The MAGMASOFT simulation predicts larger porosity in Region B in this particular lever arm. By following the procedure of Appendix B, the mean radius (μ_r) of equivalent spherical defects at three internal (near surface) locations 1, 2, and 3, sketched in Fig. 10, are estimated to be 14.4 mm, 5.5 mm, and 11.5 mm, respectively. The 10% coefficient of variation and lognormal distribution of r were defined arbitrarily.

Table 8 presents predicted failure probabilities at locations 1, 2, and 3, calculated with and without considering casting-induced shrinkage porosity. Results suggest that the presence of defect can alter failure probability by 3–4 orders of magnitude. It is interesting to note that the largest failure probability of 0.0782, which occurs in Region B due to the presence of defect, has now become larger than the largest failure probability of 0.0127 in Region A. In other words, larger failure probability may occur at other seemingly non-critical regions when casting-induced defects are considered. Therefore, mechanical fatigue
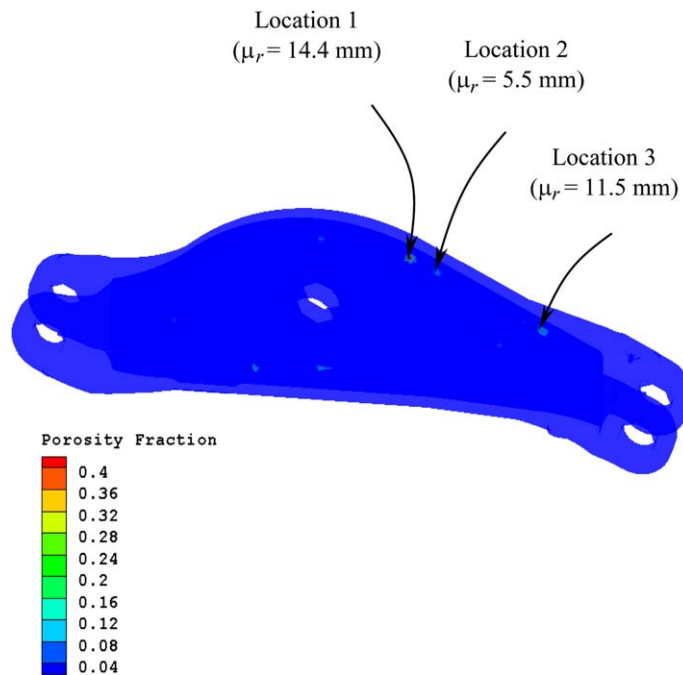

Fig. 10. Porosity field of lever arm from casting simulation.

Table 8
Probability of fatigue failure of lever arm at locations 1–3

Location	Mean defect radius, mm	Probability of fatigue failure	
		Without defect[a]	With defect[b]
1	14.4	3.396×10^{-6}	2.829×10^{-2}
2	5.5	2.294×10^{-5}	7.818×10^{-2}
3	11.5	3.433×10^{-6}	2.779×10^{-2}

[a] Random input vector: $\boldsymbol{X} = \{\sigma_f', b, \varepsilon_f', c\}^T \in \mathbb{R}^4$.
[b] Random input vector: $\boldsymbol{X} = \{\sigma_f', b, \varepsilon_f', c, S_u, r\}^T \in \mathbb{R}^6$.

design processes that do not account for casting-induced defects may neither improve design nor provide a truly reliable solution.

7. Conclusions

A new univariate method employing the most probable point as the reference point was developed for predicting failure probability of structural and mechanical systems subject to random loads, material properties, and geometry. The method involves novel decomposition at the most probable point that facilitates a univariate approximation of a general multivariate function, response surface generation of the univariate function, and Monte Carlo simulation. In addition to the effort of identifying the most probable point, the method requires a small number of exact or numerical evaluations of the performance function at selected input. Four numerical examples involving mathematical functions and structural/solid-mechanics problems illustrate the proposed method. Comparisons were made with alternative approximate and simulation methods to evaluate the accuracy and computational efficiency of the univariate method developed. Results indicate that the proposed method provides accurate and computationally efficient estimates of probability of failure. Finally, the fatigue failure of lever arm in a wheel loader was evaluated, demonstrating the ability of the new method in solving industrial-scale fatigue reliability problems.

Appendix A. Approximate evaluations of σ_m and $\Delta\varepsilon$

For a uniaxial stress state, let S_{max}, ΔS, e_{max}, and Δe denote elastically calculated maximum stress, stress range, maximum strain, and strain range at an arbitrary point, which are typically evaluated using linear-elastic FEM. Define σ_{max}, $\Delta\sigma$, ε_{max}, and $\Delta\varepsilon$ as maximum stress, stress range, maximum strain, and strain range at the same point that are evaluated using appropriate elastic–plastic analysis. Using Neuber's rule and linear-elastic calculations, the inelastic maximum stress σ_{max} and inelastic strain range $\Delta\varepsilon$ can be estimated by solving the following two pairs of equations (Stephens et al., 2001).

$$\sigma_{max}\varepsilon_{max} = K_f^2 S_{max} e_{max},$$
$$\varepsilon_{max} = \frac{\sigma_{max}}{E} + \left(\frac{\sigma_{max}}{K'}\right)^{1/n'} \tag{A.1}$$

and

$$\Delta\sigma\,\Delta\varepsilon = K_f^2\,\Delta S\,\Delta e,$$
$$\Delta\varepsilon = \frac{\Delta\sigma}{E} + 2\left(\frac{\Delta\sigma}{2K'}\right)^{1/n'}, \tag{A.2}$$

respectively, where $K' = \sigma_f'/\varepsilon_f'^{b/c}$ and $n' = b/c$ are Ramberg–Osgood parameters,

$$K_f = \begin{cases} 1, & \text{without defect,} \\ 1 + \dfrac{K_t + 1}{1 + a/r}, & \text{with defect} \end{cases} \tag{A.3}$$

is the fatigue notch factor, $K_t = 2.05$ is the elastic stress concentration factor due to a spherical notch, and $a = 0.0274(2070/S_u)^{1.8}$ with S_u in MPa and a in mm (Stephens et al., 2001). The inelastic mean stress can be easily estimated from $\sigma_m = \sigma_{max} - \Delta\sigma/2$. For a multiaxial stress state, the simplest approach involves following the same procedure using von Mises equivalent stresses and strains. Note that there are other rules, such as linear rule, Glinka's strain energy density rule, for estimating inelastic stresses and strains (Stephens et al., 2001). They were not considered in this study.

Appendix B. Porosity field and defect size

Casting simulation codes, such as MAGMASOFT (2002), are currently available that allow the size and location of shrinkage discontinuities to be predicted before a mechanical component is actually cast. Consider a three-dimensional mechanical component with physical domain $\Omega \subset \mathbb{R}^3$ and a small subdomain $\Omega_x \subset \Omega$ in the vicinity of a spatial point $x \in \Omega \subset \mathbb{R}^3$. If $p(x)$ represents the porosity field over Ω_x, the equivalent mean radius μ_r of a spherical hole (i.e., with porosity = 1) can be obtained from

$$\mu_r = \left[\frac{3 \int_{\Omega_x} p(x)\, \mathrm{d}x}{4\pi} \right]^{1/3}. \tag{B.1}$$

Using Eq. (B.1) and predicted porosity field from casting simulation, the mean size of a casting-induced defect can be estimated.

References

ABAQUS, 2002. User's Guide and Theoretical Manual, Version 6.3. Hibbitt, Karlsson, and Sorenson, Inc., Pawtucket, RI.

Anderson, T.L., 1995. Fracture Mechanics: Fundamentals and Applications, second ed. CRC Press Inc., Boca Raton, Florida.

Bjerager, P., 1988. Probability integration by directional simulation. ASCE Journal of Engineering Mechanics 114 (8), 1285–1302.

Boresi, A.P., Schmidt, R.J., 2003. Advanced Mechanics of Materials, sixth ed. John Wiley & Sons, Inc., New York, NY.

Breitung, K., 1984. Asymptotic approximations for multinormal integrals. ASCE Journal of Engineering Mechanics 110 (3), 357–366.

Cai, G.Q., Elishakoff, I., 1994. Refined second-order reliability analysis. Structural Safety 14, 267–276.

Der Kiureghian, A., Dakessian, T., 1998. Multiple design points in first and second-order reliability. Structural Safety 20 (1), 37–49.

Ditlevsen, O., Madsen, H.O., 1996. Structural Reliability Methods. John Wiley & Sons Ltd., Chichester.

Grandhi, R., Wang, L., 1999. Higher-order failure probability calculation using nonlinear approximations. Computer Methods in Applied Mechanics and Engineering 168, 185–206.

Hohenbichler, M., Gollwitzer, S., Kruse, W., Rackwitz, R., 1987. New light on first- and second-order reliability methods. Structural Safety 4, 267–284.

Madsen, H.O., Krenk, S., Lind, N.C., 1986. Methods of Structural Safety. Prentice-Hall, Inc., Englewood Cliffs, NJ.

MAGMASOFT, 2002. User Manual. MAGMA Foundry Technology Inc., Arlington Heights, IL.

Nie, J., Ellingwood, B.R., 2000. Directional methods for structural reliability analysis. Structural Safety 22, 233–249.

Penmetsa, R., Grandhi, R., 2003. Adaptation of fast Fourier transformations to estimate structural failure probability. Finite Elements in Analysis and Design 39, 473–485.

Rackwitz, R., 2001. Reliability analysis—a review and some perspectives. Structural Safety 23 (4), 365–395.

Stephens, R.I., Fatemi, A., Stephens, R.R., Fuchs, H.O., 2001. Metal Fatigue in Engineering, second ed. John Wiley & Sons, Inc., New York, NY.

Tvedt, L., 1990. Distribution of quadratic forms in normal space—application to structural reliability. ASCE Journal of Engineering Mechanics 116 (6), 1183–1197.

Xu, H., Rahman, S., 2004. A generalized dimension-reduction method for multi-dimensional integration in stochastic mechanics. International Journal for Numerical Methods in Engineering 61, 1992–2019.

Xu, H., Rahman, S., accepted for publication. Decomposition methods for structural reliability analysis. Probabilistic Engineering Mechanics.

Yau, J.F., Wang, S.S., Corten, H.T., 1980. A mixed-mode crack analysis of isotropic solids using conservation laws of elasticity. Journal of Applied Mechanics 47, 335–341.